cis Donor Influence on O-O Bond Lability in Iron(III) Hydroperoxo Complexes

Wegeberg, Christina; Browne, Wesley R.; McKenzie, Christine J.

IMPORTANT NOTE: You are advised to consult the publisher's version (publisher's PDF) if you wish to cite from it. Please check the document version below.

Document Version
Publisher's PDF, also known as Version of record

Link to publication in University of Groningen/UMCG research database

cis Donor Influence on O−O Bond Lability in Iron(III) Hydroperoxo Complexes: Oxidation Catalysis and Ligand Transformation

Christina Wegeberg,[†,‡] Wesley R. Browne,[‡] and Christine J. McKenzie[*,†]

[†]Department of Physics, Chemistry and Pharmacy, University of Southern Denmark, Campusvej 55, 5230 Odense M, Denmark
[‡]Molecular Inorganic Chemistry, Stratingh Institute for Chemistry, University of Groningen, Nijenborgh 4, 9747 AG Groningen, The Netherlands

S Supporting Information

ABSTRACT: The Fe^{III}/Fe^{II} redox potentials for $[Fe(tpen)]^{2+/3+}$, $[Fe(tpena)]^{+/2+}$, and $[Fe(tpenO)]^{+/2+}$ (N-R-N,N′,N′-tris(2-pyridylmethyl)ethane-1,2-diamine, where R = $CH_2C_6H_4N$, CH_2COO^-, $CH_2CH_2O^-$, respectively) span 470 mV with the oxidation potentials following the order $[Fe^{II}(tpenO)]^+$ (MeOH) < $[Fe^{II}(tpena)]^+$ (MeCN) < $[Fe^{II}(tpen)]^{2+}$ (MeCN). In their +3 oxidation states the complexes react with 1 equiv of H_2O_2 to give the purple $[Fe^{III}(OOH)(HL)]^{n+}$ (n = 2 for L = tpena, tpenO; n = 3 for L = tpen). A pyridine arm is decoordinated in these complexes, furnishing a second coordination sphere base which is protonated at ambient pH. The lifetimes of these transient species depend on how readily the substrate (sometimes the solvent) is oxidized and reflect the trend in both the O−O bond lability and oxidizing potency of the putative iron-based oxidant derived from the iron(III) peroxides. In methanol solution, $[Fe^{III}(tpenO)]^{2+}$ and $[Fe^{III}(tpena)]^{2+}$ exist in their Fe(III) states and hence the formation of $[Fe^{III}(OOH)(Htpena)]^{2+}$ and $[Fe^{III}(OOH)(HtpenO)]^{2+}$ is instantaneous. This is in contrast to the short lag time that occurs before adduct formation between $[Fe^{II}(tpen)]^{2+}$ and H_2O_2 due to the requisite prior oxidation of the solution-state iron(II) complex to its iron(III) state. Stabilization of the +3 iron oxidation state in the resting state catalysts affords complexes that activate H_2O_2 more readily with the consequence of higher yields in the oxidation of the C−H bonds using H_2O_2 as terminal oxidant. The presence of a cis monodentate carboxylato donor increases the rate of oxidation by hydrogen atom transfer in comparison to the systems with an alkoxo or pyridine in this position. Competing with substrate oxidation is the oxidative modification of the alkoxido group in $[Fe^{III}(tpenO)]^{2+}$, converting it to a carboxylato group in the presence of H_2O_2: in effect, transforming tpenO to tpena.
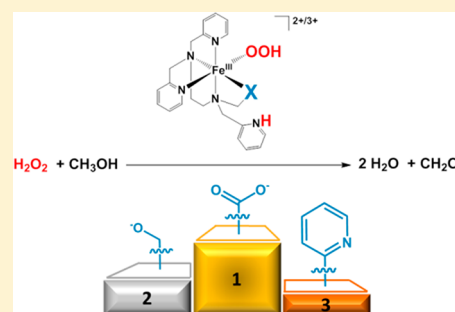
■ INTRODUCTION

The active sites of otherwise related metalloenzymes are tuned by the first and second coordination spheres according to their precise function.[1−9] The switch between reversible O_2 binding and its irreversible activation is effected by the ligand axial to the O_2 binding site in myoglobin vs the related heme site of cytochrome P450. These axial ligands, histidine and cysteine, respectively, modulate the electron donation to the iron center, affecting the basicity of the iron(IV) hydroxide, which is crucial for the catalytic function of the enzymes.[10−12] In the nonheme iron enzyme class a similar trend is observed: e.g., in hemerythrin and soluble methane monooxygenase (sMMO) the switch from reversible binding of dioxygen to its activation is predominantly effected by the replacement of histidine donors by more electron rich carboxylato donors (Scheme 1a).[13,14] These are approximately cis to the O_2 binding site.[15−17] O−O bond cleavage of the coordinated dioxygen generates a high-valent bis(μ-oxo)iron(IV) intermediate (Q) in sMMO capable of the selective hydroxylation of the strong C−H bond of alkanes.[18−22] With the cooperation of redox-active organic cofactors, mononuclear nonheme enzymes, which contain a carboxylato donor also cis to the O_2 binding site, can similarly generate high-valent iron-based oxidants

from O_2 for the selective hydroxylation of C−H bonds.[23,24] An example is the TauD species J for α-ketoglutarate (α-KG)-dependent dioxygenases (Scheme 1b).[25−28] In contrast the mononuclear nonheme iron enzyme lipoxygenase does not directly activate O_2 or peroxides; instead, the catalytic regio- and stereospecific hydroperoxidation of 1,4-(Z,Z)-pentadiene-containing polyunsaturated carboxylic acids is initiated by H atom abstraction from the lipid substrate by a $Fe^{III}OH$ species.[29−31] The carboxylato donor (terminal isoleucine) for the iron center cis to the reactive hydroxide ligand is undoubtedly integral for maintaining the requisite iron(III) oxidation state and ensuring the presence of a hydroxo rather than a water ligand.

Systematic investigations of the influence of supporting ligands on the reactivity of nonheme iron model compounds have previously been reported in the literature.[34−37] Tris-2-pyridylmethylamine (TPA) supports a low-spin iron(III) hydroperoxo complex; however, a high-spin iron state is stabilized by methyl substitution at the 6′-position of the pyridyls.[35] The catalytic capabilities of $[Fe^{II}(TPA)(MeCN)]^{2+}$

Scheme 1. Structurally Related Active Sites of Diiron and Monoiron Non-Heme Iron Enzymes in Their Iron(II) States: (a) Hemerythrin (1HMD)[15] and Methane Monooxygenase (1MMO)[16] and (b) α-KG-Dependent Dioxygenase (1GQW)[32] and Lipoxygenase (1YGE)[33]

(a) Hemerythrin

Methane Monooxygenase

(b) α-Ketoglutarate dependent dioxygenase

Lipoxygenase
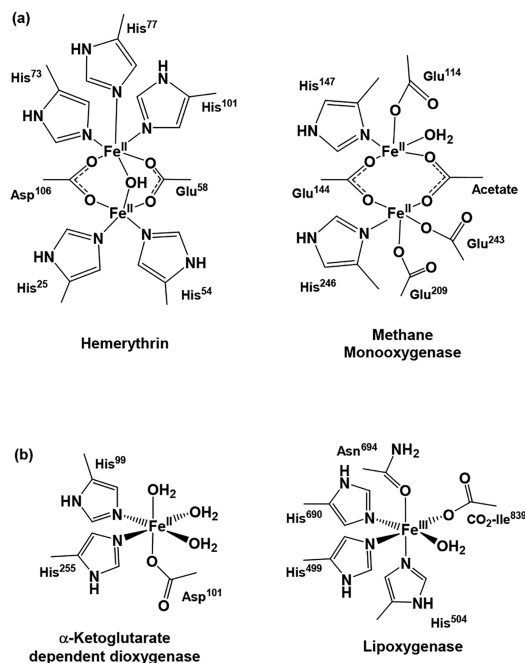
and $[Fe^{II}(6\text{-}Me_3TPA)(MeCN)]^{2+}$ in the oxidation of cyclooctene by H_2O_2 show that the methylation of the pyridine donors effects a change in the distribution of the epoxide to diol products from 1:1.2 to 1:7.[38] In this case the N donors of the first coordination sphere scaffold are identical. Efforts to assess the influence of the first coordination sphere have focused on the use of exchangeable monodentate coligands. Variation of the ligand *cis* to the oxo group in $[Fe^{IV}O(TPA)(X)]^{2+/+}$ (X = MeCN, OTf⁻, Cl⁻, Br⁻) results in a change in near-IR absorption (720−800 nm), but not in the Fe−O bond length, Mössbauer parameters, or the energy of the X-ray absorption pre-edge.[36] A *trans* influence is evident in variation of the donor X *trans* to the $Fe^{IV}=O$ moiety in $[Fe^{IV}O(TMC)(X)]^{2+}$ (TMC = 1,4,8,11-tetramethyl-1,4,8,11-tetraazacyclotetradecane, X = MeCN, HO⁻, N₃⁻, CN⁻, OCN⁻, SCN⁻, OTf⁻), and it is manifested in the near-IR absorption spectra, $\nu_{Fe=O}$ stretching frequencies, Mössbauer quadrupole splitting parameters, and XAS pre-edge intensities.[37] The activity of $[Fe^{IV}O(TMC)(X)]^{2+}$ (X = MeCN, OTf⁻, N₃⁻) and the related complex $[Fe^{IV}O(TMCS)]^{2+}$ [39] (a methyl group of TMC is replaced with a pendant chelating ethanethiolato) in hydrogen atom transfer (HAT) reactions of the O−H and C−H bonds of phenol, alkyl, and aromatic molecules, respectively, has revealed that the most reactive species is the iron(IV) oxo complex $[Fe^{IV}O(TMCS)]^{2+}$,[40] which incidentally shows the lowest Fe^{3+}/Fe^{2+} reduction potential.

Nonheme iron(III) hydroperoxo and peroxo complexes supported by ethylenediamine-backboned ligands, $[Fe^{III}(OOH)(Rtpen)]^{2+}$ and $[Fe^{III}(OO)(Rtpen)]^+$ (Rtpen = *N*-R-*N*,*N*′,*N*′-tris(2-pyridylmethyl)ethane-1,2-diamine, R = Me, Et, iPr, Bz, Ph, 2-methylpyridyl), have been known for over two decades.[41−44] The R groups in Rtpen are typically noncoordinating alkyl or benzyl groups, and thus Rtpen ligands

furnish N5 donor coordination spheres. $[Fe^{III}(OOH)(Rtpen)]^{2+}$ complexes are stable enough to be observable at room temperature in methanol for seconds to hours. In fact, they are quite often best observed in methanol. The replacement of a 2-methylpyridyl or the alkyl R group in the Rtpen scaffold with potentially chelating arms offers the possibility of investigation of the influence of different chelating donors *cis* to a reactive hydroperoxide ligand in their iron complexes. The introduction of a carboxylato group is particularly interesting due to the aforementioned relevance to the first coordination sphere of nonheme iron enzymes. We have introduced glycyl groups to give the related ethylenediamine-based ligands *N*-R-*N*,*N*′-bis(2-pyridylmethyl)-ethylenediamine-*N*′-acetate (Rbpena, R = methyl, benzyl, N4O ligand)[45] and *N*,*N*,*N*′-tris(2-pyridylmethyl)-ethylenediamine-*N*′-acetate (tpena, N5O ligand, Scheme 2a).[46] With their chelating single monodentate carboxylate donor, these modifications to the Rtpen (R = Me, Bz) and tpen ligands, respectively, influence dramatically the oxidant activation chemistry of their iron complexes in comparison to the neutral N5 Rtpen and N6 tpen supported systems. Depending on the N4O or N5O ligand and the solvent, these complexes show reactivity patterns that mimic the wide range of reactivities shown by the mononuclear nonheme enzymes: for example, regioselective ligand oxygenation at the phenyl moiety or the amine by O_2, HOOH, and ROOH,[45] catalysis of sulfoxidation and epoxidation with PhIO,[47,48] and the catalytic disproportionation of H_2O_2[46] and ROOH.[49]
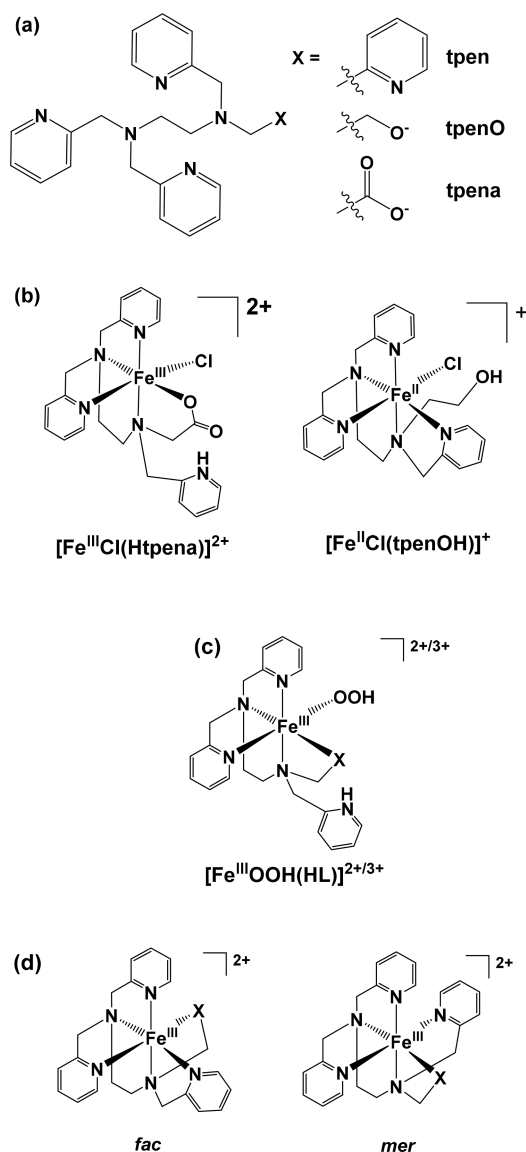
Ligands with an ethylenediamine backbone tetrasubstituted with four donor arms can furnish an important biomimetic feature: ligand flexibility. They allow for hepta- or hexacoordination of the metal ion on adduct formation with a monodentate exogenous donor. The latter occurs through decoordination of a donor arm, which can then act as second coordination sphere base. In the systems described here for the iron(III) oxidation state, this is always a pyridine arm.[47,49,50] The N5O tpena ligand scaffold is a significant contribution for the modeling of nonheme iron enzymes, since the majority of nonheme iron models do not provide either a *cis* monodentate carboxylato donor or a second coordination sphere base. Both the carbonyl of the carboxylate donor and the dangling pyridine have inherent potential for participating in H-bonding and proton transfer.

Here we describe a comparative study of the H_2O_2 activation chemistry of iron complexes with flexible ethylenediamine-based N6 and N5O hexadentate ligands (when fully coordinated), where one arm is either a 2-methylpyridyl (tpen), an ethoxide (tpenO), or a glycyl group (tpena) (Scheme 2a). The spectroscopic characterization of the iron(III) peroxo species[46,51,52] has been extended and includes experiments which enable a direct comparison of the stability and reactivity of these complexes. Ultimately our results show that the evolution from a pyridine donor or an alkoxido to a carboxylato donor in the position *cis* to a hydroperoxide coligand in an iron(III) complex increases the propensity for homolytic cleavage of the FeO−OH bond.

■ RESULTS AND DISCUSSION

Tpen, tpena, and tpenO can act as penta- or hexadentate ligands. In the case of pentacoordination an uncoordinated donor can be protonated (Scheme 2c). We have coined abbreviations for the complexes of these ligands to reflect as far as possible the site of protonation (Figure S1). Thus, the

Scheme 2. (a) General Chemical Structures of the Ethylenediamine Backboned Ligands tpen = N,N,N',N'-Tetrakis(2-pyridylmethyl)ethylenediamine, tpenO = N,N,N'-Tris(2-pyridylmethyl)ethylenediamine-N'-ethoxido, and tpena = N,N,N'-Tris(2-pyridylmethyl)ethylenediamine-N'-acetate. (b) Structures of Known Mononuclear Iron(III) and Iron(II) Complexes of Htpena and tpenOH, Respectively, (c) Structure of the Proposed Dominant Diastereoisomer of the Charge-Separated H_2O_2 Adducts of the Iron(III) Complexes of $[Fe^{III}(tpen)]^{3+}$, $[Fe^{III}(tpenO)]^{2+}$, and $[Fe^{III}(tpena)]^{2+}$ with X = py, Ethoxido, Glycylato, and (d) Structures of Diastereoisomers of $[Fe^{III}(tpenO)]^{2+}$ and $[Fe^{III}(tpena)]^{2+}$

(a)

X = tpen

O⁻ tpenO

O⁻ tpena

(b)

$[Fe^{III}Cl(Htpena)]^{2+}$　　　$[Fe^{II}Cl(tpenOH)]^{+}$

(c)

$[Fe^{III}OOH(HL)]^{2+/3+}$

(d)

fac　　　*mer*

alcohol of tpenOH remains protonated and is uncoordinated in $[Fe^{II}Cl(tpenOH)]^{+}$, where the ligand is pentadentate (Scheme 2b). If the alcohol group of tpenOH is deprotonated, it is an alkoxido donor and the ligand is hexadentate. The complex is named $[Fe^{III}(tpenO)]^{2+}$ (Scheme 2d). In complexes where a pyridine arm is uncoordinated and protonated, while the O donor is coordinated and deprotonated, the abbreviated ligand names in the complex are formulated as Htpena and HtpenO. The abbreviated names are

illustrated with the crystallographically characterized iron chlorides $[Fe^{III}Cl(Htpena)]^{2+}$ and $[Fe^{II}Cl(tpenOH)]^{+}$ (Scheme 2b).[46,52]

Solution-State Chemistry of $[Fe^{II}Cl(tpenOH)]^{+}$ and *fac*- and *mer*-$[Fe^{III}(tpenO)]^{2+}$. Solution-state mononuclear $[Fe(tpen)]^{n+}$ (n = 2, 3) complexes are obtained upon dissolution of the simple salts $[Fe(tpen)](PF_6)_2$ and $[Fe(tpen)](ClO_4)_{2/3}$.[53,54] Access to the solution-state complexes $[Fe^{III}(tpenO)]^{2+}$ and $[Fe^{III}(tpena)]^{2+}$ is less straightforward. $[Fe^{III}(tpena)]^{2+}$ is obtained through the dehydration of the hemihydrate cation in $[Fe^{III}_2O(Htpena)_2](ClO_4)_4$, which occurs spontaneously over the course of a few minutes on dissolution in acetonitrile.[48,55] As a N5O-supported ligand system, $[Fe^{III}(tpena)]^{2+}$ is diastereoisomeric (Scheme 2d). We have previously spectroscopically characterized *fac*-$[Fe^{III}(tpena)]^{2+}$ (S = 1/2, g = 2.74, 2.29, 1.68, δ = 0.16 mm s⁻¹, ΔE_Q = 2.17 mm s⁻¹) and *mer*-$[Fe^{III}(tpena)]^{2+}$ (S = 5/2, g^{eff} = 4.2, δ = 0.31 mm s⁻¹) in both the solid and solution states and the less reactive *fac*-$[Fe^{III}(tpena)]^{2+}$ has also been structurally characterized.[48] $[Fe^{III}(tpenO)]^{2+}$ has not previously been reported; however, in analogy to $[Fe^{III}(tpena)]^{2+}$ diastereoisomers can be expected.

Solid- and solution-state IR spectra (Figure 1) are useful for identifying the distinguishing structural features of the cations in $[Fe^{II}(tpen)](PF_6)_2$, $[Fe^{II}Cl(tpenOH)]PF_6$, $[Fe^{III}_2O-(Htpena)_2](ClO_4)_4$, and their mononuclear acetonitrile solution state derivatives, $[Fe^{II}(tpen)]^{2+}$, $[Fe^{II}Cl(tpenOH)]^{2+}$, and $[Fe^{III}(tpena)]^{2+}$. In agreement with the noncoordinated alcohol arm found in the crystal structure of $[Fe^{II}Cl-(tpenOH)]PF_6$, an O−H vibration is observed at 3418 cm⁻¹ in the solid-state IR spectrum (Figure 1a, blue). Intense bands at 1073 and 1660 cm⁻¹ for $[Fe^{III}_2O(Htpena)_2](ClO_4)_4$ are due to the C−O and C=O stretches, respectively, of the carboxylato donor. The solution-state (d_3-MeCN) IR spectrum of $[Fe^{III}_2O(Htpena)_2](ClO_4)_4$ shows that it has partially dehydrated to give the mononuclear $[Fe^{III}(tpena)]^{2+}$, since intense bands can be seen at both 1675 and 1715 cm⁻¹ for the C=O stretches of $[Fe^{III}_2O(Htpena)_2)]^{4+}$ and $[Fe^{III}(tpena)]^{2+}$. Solution-state Mössbauer spectroscopy of a similarly prepared solution consistently showed that $[Fe^{III}_2O(Htpena)_2)]^{4+}$ and $[Fe^{III}(tpena)]^{2+}$ coexist in acetonitrile.[55] The relative concentrations will depend on the concentration of water, with higher water content increasing the concentration of $[Fe^{III}_2O-(Htpena)_2)]^{4+}$.

Solution-state EPR spectra of $[Fe^{II}Cl(tpenOH)]PF_6$ dissolved in MeOH shows that samples, which are frozen immediately after dissolution, do not exhibit an EPR signal at 100 K. This is consistent with the iron(II) oxidation state that is present in the solid starting material. However, if the solution is frozen 10 min after dissolution, two rhombic low-spin iron(III) signals (g = 2.33, 2.15, 1.93 and g = 2.40, 2.17, 2.00; Figure 2a) can be deconvoluted from the EPR spectrum. This shows that in methanol solution the solid-state precursor in $[Fe^{II}Cl(tpenOH)]^{+}$ is oxidized by air over the course of minutes. Oxidation to the +3 state increases the oxophilicity of the iron atom, and binding and deprotonation of the ethanol arm to form $[Fe^{III}(tpenO)]^{2+}$ as the major solution species occur (Scheme 3, *fac*-py₃ isomer shown).

The appearance of two rhombic signals in the EPR spectrum is consistent with the formation of diastereoisomers: *fac*-py₃-$[Fe^{III}(tpenO)]^{2+}$ and *mer*-py₃-$[Fe^{III}(tpenO)]^{2+}$. Thus, in contrast to the tpena-supported system,[48] both of the diastereoisomers of $[Fe^{III}(tpenO)]^{2+}$ are low spin (S = 1/2).
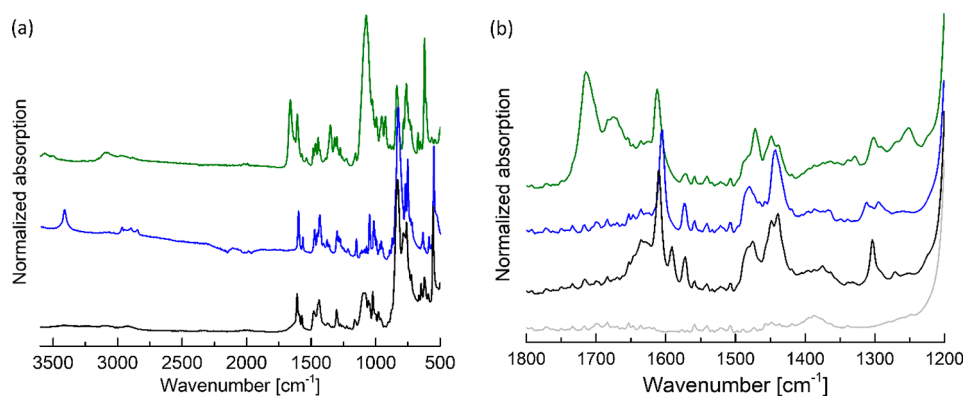
**Figure 1.** FTIR spectra of $[Fe^{II}(tpen)](PF_6)_2$ (black), $[Fe^{II}Cl(tpenOH)]PF_6$ (blue), and $[Fe^{III}_2O(Htpena)_2](ClO_4)_4$ (green) (a) in the solid state and (b) in solution (d_3-MeCN), where the speciation is $[Fe^{II}(tpen)]^{2+}$ (black), $[Fe^{II}Cl(tpenOH)]^+$ (blue), and $[Fe^{III}(tpena)]^{2+}$ (green). The spectrum of d_3-MeCN is shown in gray.
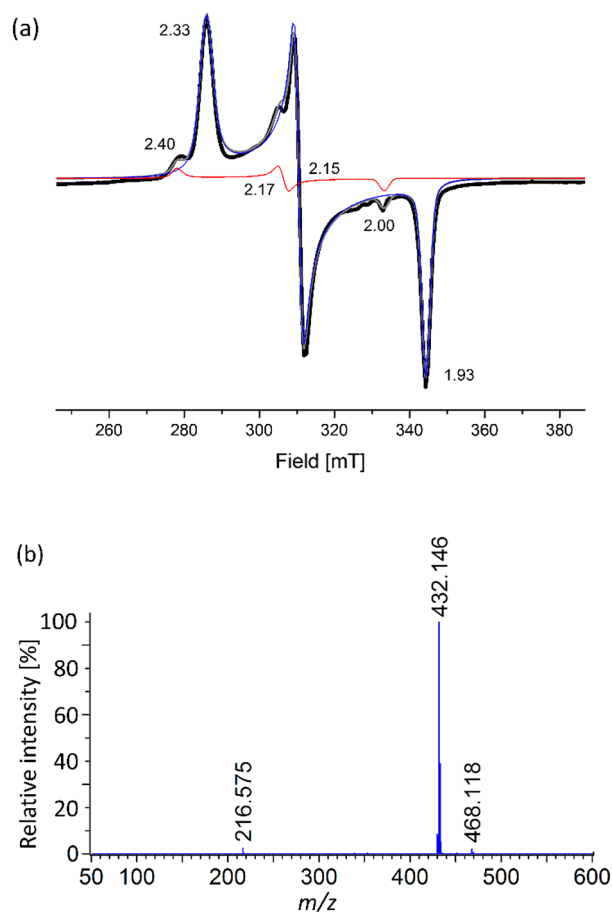
Figure 2. (a) X-band EPR (black, 100 K, [Fe] = 3 mM, microwave frequency 9.32599 GHz) spectrum of $[Fe^{II}Cl(tpenOH)]PF_6$ dissolved in MeOH and frozen 10 min after dissolution. The two rhombic low-spin iron(III) signals are simulated in red and blue, and the sum of the fitted spectra is shown in gray. (b) ESI-MS spectrum of $[Fe^{II}Cl$-$(tpenOH)]PF_6$ (MeCN, positive mode). Assignment of ions: m/z 216.575 $[Fe^{II}(tpenOH)]^{2+}$ ($C_{22}H_{27}FeN_5O$ calcd 216.578), 432.146 $[Fe^{II}(tpenO)]^+$ ($C_{22}H_{26}FeN_5O$ calcd 432.148), and 468.118 $[Fe^{II}(tpenOH)Cl]^+$ ($C_{22}H_{27}ClFeN_5O$ calcd 468.125).

However, the intensities of the EPR signals for fac-$[Fe^{III}(tpenO)]^{2+}$ and mer-$[Fe^{III}(tpenO)]^{2+}$ indicate that they are present in unequal amounts. Given the axial juxtaposition of the three pyridines and the three hard σ-donors as well as

Scheme 3. Spontaneous Oxidation of $[Fe^{II}Cl(tpenOH)]^+$ to $[Fe^{III}(tpenO)]^{2+}$ in Methanol under Ambient Conditions
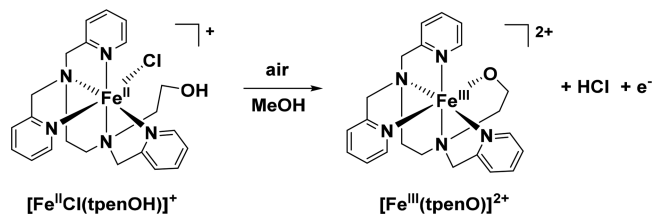
the starting conformation in the single-crystal X-ray structure of the precursor $[Fe^{II}Cl(tpenOH)]PF_6$, we deduce that fac-$[Fe^{III}(tpenO)]^{2+}$ is likely to be the most stable isomer and therefore the major species in solution. fac-$[Fe^{III}(tpenO)]^{2+}$ formation requires just a direct substitution of the chloride by the alkoxide arm of $[Fe^{II}Cl(tpenOH)]^+$ (Scheme 3). Stereochemical support is furnished by the fact that the related fac isomer is dominant in solutions of $[Fe^{III}(tpena)]^{2+}$.[48,55] The ESI-MS spectrum of an acetonitrile solution prepared from $[Fe^{II}Cl(tpenOH)]PF_6$ (Figure 2b) shows a monocationic base peak of m/z 432.146, which can be assigned to $[Fe^{II}(tpenO)]^+$. Low-intensity ions can be assigned to its protonated adduct, $[Fe^{II}(tpenOH)]^{2+}$. Significantly, only a trace of $[Fe^{II}Cl$-$(tpenOH)]^+$ is detected. The addition of excess NH_4Cl does not change the ion distribution, suggesting that the chelating alkoxy arm efficiently outcompetes chloride coordination. In methanol no chloride-containing complex is detected. Dissolution of $[Fe^{II}Cl(tpenOH)]PF_6$ produces yellow solutions with a maximum absorbance band at either 393 nm (ε = 2000 M^{-1} cm^{-1}) or 398 nm (2100 M^{-1} cm^{-1}) in methanol and acetonitrile, respectively.

A reversible Fe^{III}/Fe^{II} redox wave appears at -0.08 V vs $Fc^+/$ Fc (Figure 3 and Figure S2) in the cyclic voltammogram (CV) for the solution-state $[Fe^{III}(tpenO)]^{2+}$ derived from the solid-state $[Fe^{II}Cl(tpenOH)]PF_6$ in methanol. In acetonitrile a reversible wave at 0.17 V vs Fc^+/Fc appears in the CV of $[Fe^{II}Cl(tpenOH)]PF_6$. The 250 mV difference is consistent with N5O and N5Cl coordination spheres in methanol and acetonitrile, respectively. For comparison the reversible $Fe^{III}/$ Fe^{II} redox waves for $[Fe^{II}(tpen)]^{2+}$ and $[Fe^{III}(tpena)]^{2+}$ appear at 0.39 and 0.04 V in acetonitrile.[46] The minor reduction wave at -0.08 V in the CV of $[Fe^{II}Cl(tpenOH)]PF_6$ in acetonitrile is due to traces of $[Fe^{III}(tpenO)]^{2+}$. These data are consistent with the expectation that coordination of a negatively charged
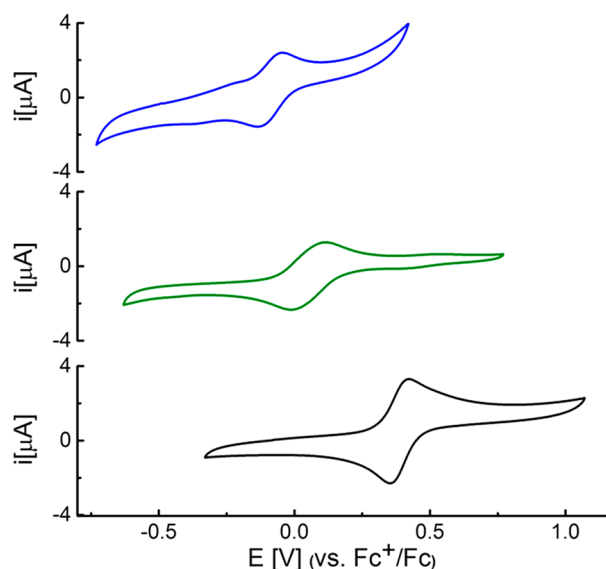
**Figure 3.** Cyclic voltammograms of $[Fe(tpen)](PF_6)_2$ (black) and $[Fe_2O(Htpena)_2](ClO4)_4$ (green) dissolved in acetonitrile containing 0.1 M TBAClO$_4$ and $[FeCl(tpenOH)]PF_6$ (blue) dissolved in methanol containing 0.1 M TBAClO$_4$. The bulk solution speciation is $[Fe^{II}(tpen)]^{2+}$, $[Fe^{III}(tpena)]^{2+}$, and $[Fe^{III}(tpenO)]^{2+}$, respectively. Conditions: [Fe] = 0.5 mM, scan rate 100 mV s^{-1}.

alkoxido or carboxylato donor in place of a pyridyl moiety will stabilize the higher iron oxidation state. Consistently the Fe^{3+} oxidation state is clearly favored for the two N5O ligands (O = alkoxido, carboxylato) when they are fully deprotonated and coordinated in the hexadentate mode. The relatively large span of 470 mV in Fe^{III}/Fe^{II} redox potentials for the series $[Fe^{II}(tpen)]^{2+}$, $[Fe^{II}Cl(tpenOH)]^+$, $[Fe^{III}(tpena)]^{2+}$, and $[Fe^{III}(tpenO)]^{2+}$ (charge formulation in accord with the most stable oxidation state in solution) supports the expected trends produced by N6, N5Cl, N5O(carboxylato), and N5O(alkoxide) first coordination spheres. The span in this series is significantly greater than the 15 mV shown for the reversible Fe^{III}/Fe^{II} redox couples for $[Fe(tpen)]^{2+}$ and an tetraethylated derivative.[56]

Transient $[Fe^{III}OOH(HtpenO)]^{2+}$ and $[Fe^{III}OO-(HtpenO)]^+$. A purple iron(III) hydroperoxo species is formed on the addition of H$_2$O$_2$ to $[Fe^{II}Cl(tpenOH)]PF_6$ dissolved in MeOH.[52] This intermediate has previously been characterized only by its electronic absorption (λ_{max} = 537 nm) and was formulated as $[Fe^{III}(OOH)(tpenOH)]^{2+}$ by analogy with the

structurally characterized dangling ethanol arm of its iron(II) precursor, $[Fe^{II}Cl(tpenOH)]PF_6$.[52] It was noted, however, that this species distinguished itself by showing a significantly shorter half-life in comparison to the N5 ethylenediamine ligand-based systems $[Fe^{III}(OOH)(Rtpen)]^{2+}$, where the R group was an alkyl or aryl and contained no heteroatoms (minutes vs several hours) and that there was no lag time for its formation. The present reinvestigation, which includes further spectroscopic studies, now explains the lack of lag time: the complex is preoxidized just by its dissolution in methanol. Thus, formation of a "charge-separated" adduct (HOO$^-$ coordinates to the iron(III) and a pyridine group is decoordinated and protonated; eq 1 and Scheme 2c) of $[Fe^{III}(tpenO)]^{2+}$ with H$_2$O$_2$ is more facile in comparison with the reactions of H$_2$O$_2$ with $[Fe^{II}Cl(Rtpen)]^+$ (R = Me, Et, iPr, Bz, Ph)[52] and $[Fe(tpen)]^{2+}$, which encompass a separated metal oxidation step and a ligand substitution step. A lag time for the formation of $[Fe^{III}(OOH)(Htpen)]^{3+}$ is observed even on the addition of a large excess (50 equiv) of H$_2$O$_2$ (Figure S3).

$$[Fe^{III}(tpenO)]^{2+} + H_2O_2 \rightarrow [Fe^{III}(OOH)(HtpenO)]^{2+} \tag{1}$$
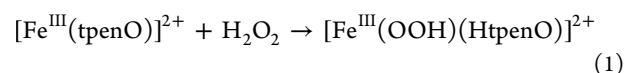
The lifetime of $[Fe^{III}(OOH)(HtpenO)]^{2+}$ is extended in CD$_3$OD in comparison to CH$_3$OH ($T_{1/2}$ = 900 s vs $T_{1/2}$ = 300 s; Figure S4). Examination of the methanol solutions containing $[Fe^{III}(OOH)(HtpenO)]^{2+}$ and excess H$_2$O$_2$ using a colorimetric test for formaldehyde (Hantzsche reaction[57]) confirms its presence, verifying that background methanol oxidation is occurring. Quantification of the formaldehyde showed 8% yield with respect to H$_2$O$_2$ concentration (50 equiv, 1.5 mM [Fe]) 15 min after the addition of H$_2$O$_2$. For comparison, only trace amounts of formaldehyde are detected in methanol solutions of $[Fe^{III}(OOH)(metpen)]^{2+}$ (metpen = N-methyl-N,N',N'-tris(2-pyridylmethyl)-1,2-diaminoethane) and $[Fe^{III}(OOH)(Htpen)]^{3+}$ under the same conditions (1 and 2%, respectively). Hence, the shorter half-life of $[Fe^{III}(OOH)(HtpenO)]^{2+}$ vs $[Fe^{III}(OOH)(Rtpen)]^{2+}$ and $[Fe^{III}(OOH)(Htpen)]^{3+}$ is explained by its rapid onward use in solvent oxidation. $[Fe^{III}(OOH)(Htpena)]^{2+}$ cannot be detected in methanol, even at low temperatures, due to greater transiency caused by an even more efficient methanol oxidation. The yield of formaldehyde using $[Fe^{III}(OOH)-(Htpena)]^{2+}$ was 35% with respect to the amount of H$_2$O$_2$ added. It is however possible to spectroscopically characterize $[Fe^{III}(OOH)(Htpena)]^{2+}$ by using acetonitrile as the solvent

Table 1. Spectroscopic Properties of Ethylenediamine Backboned Iron(III) Hydroperoxide and Peroxide Complexes with the Supporting Ligands tpen, HtpenO, and Htpena

complex	UV–visible λ_{max} (nm)	rRaman (cm^{-1})		EPR g values[a]	S	ref
		ν_{Fe-OOH}	ν_{FeO-OH}			
$[Fe(tpenO)]^{2+,b}$ (two diastereoisomers)	393	na	na	2.33, 2.15, 1.93	1/2	this work
				2.40, 2.17, 2.00	1/2	
$[Fe^{III}(OOH)(Htpena)]^{2+\,c}$	520	613	788	2.21, 2.15, 1.96	1/2	46
$[Fe^{III}(OOH)(Htpen)]^{3+\,b}$	541	617	796	2.22, 2.15, 1.97	1/2	51
$[Fe^{III}(OOH)(HtpenO)]^{2+\,b}$	537	619	800	2.21, 2.14, 1.97	1/2	52, this work
				2.25, 2.15, 2.00	1/2	
$[Fe^{III}(OO)(Htpena)]^{+\,c}$	675	473	815	8.8, 5.0, 4.3, 4.2, 3.5	5/2	46
$[Fe^{III}(OO)(HtpenO)]^{+\,b}$	716	472	818	8.0, 4.3	5/2	52, this work
$[Fe^{III}(OO)(Htpen)]^{2+\,b}$	755	470	817	7.5, 5.9	5/2	51

[a]For S = $^5/_2$ g^{eff} values are shown. [b]Recorded in MeOH. na = not applicable. [c]Recorded in MeCN.
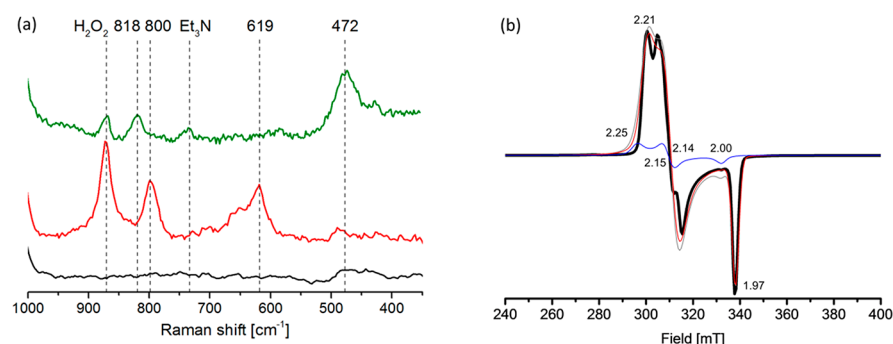
Figure 4. (a) rRaman spectra of $[Fe^{III}(tpenO)]^{2+}$ in MeOH (black) and after addition of 50 equiv of H_2O_2 to generate $[Fe^{III}(OOH)(HtpenO)]^{2+}$ (red) followed by addition of 10 equiv of Et_3N to form $[Fe^{III}(OO)(HtpenO)]^+$ (green). Conditions: -25 °C, $[Fe]$ = 3 mM, λ_{exc} = 785 nm. (b) X-band EPR spectrum of $[Fe^{III}(tpenO)]^{2+}$ in MeOH with 50 equiv of H_2O_2 (black). Conditions: 100 K, $[Fe]$ = 3 mM, microwave frequency 9.30555 GHz. Individual fitted spectra are seen in red and blue. The sum of the fitted spectra is seen in gray.

for measurement, since this solvent is less readily oxidized.[46] Another significant difference among the H_2O_2 activation properties of $[Fe^{II}(tpen)]^{2+}$, $[Fe^{III}(tpenO)]^{2+}$, and $[Fe^{III}(tpena)]^{2+}$ is noteworthy: in the absence of suitable C–H substrates, such as methanol, $[Fe^{III}(tpena)]^{2+}$ catalyzes H_2O_2 disproportionation.[46] We do not observe any sign of O_2 evolution from solutions containing $[Fe^{III}(tpenO)]^{2+}$, $[Fe^{II}(Rtpen)]^{2+}$, or $[Fe^{II}(tpen)]^{2+}$ under the same conditions ($[Fe]$ = 0.5 mM, 50 equiv of H_2O_2, acetonitrile solvent) by visual examination or using head space Raman spectroscopy as we could for the H_2O_2 disproportionation reactions with $[Fe^{III}(tpena)]^{2+}$.[46] This behavior for $[Fe^{III}(tpena)]^{2+}$ suggests higher promiscuity for this catalyst in oxidative HAT reactions in comparison to other nonheme iron-based catalysts.

The spectroscopic parameters for $[Fe^{III}(OOH)(HtpenO)]^{2+}$ are similar to those for other ethylenediamine-backboned iron(III)hydroperoxo species (Table 1). The resonance Raman spectrum of $[Fe^{III}(OOH)(HtpenO)]^{2+}$ (λ_{exc} = 785 nm) showed resonance-enhanced bands at 619 and 800 cm^{-1} (Figure 4a) assigned to ν_{Fe-O} and ν_{O-O} vibrations, respectively. The EPR spectrum of a frozen solution can be deconvoluted to show two rhombic low-spin iron(III) ($S = 1/2$) signals with g = 2.21, 2.14, 1.97 and g = 2.25, 2.15, 2.00 (Figure 4b, red and blue, respectively). Interestingly, the ratio of the spin concentrations for the EPR signals due to the two $S = 1/2$ diastereoisomers is 9:1 in the spectra of $[Fe^{III}(tpenO)]^{2+}$ (Figure 2a) and $[Fe^{III}(OOH)(HtpenO)]^{2+}$ (Figure 4b). This suggests that *fac*- and *mer*-$[Fe^{III}(tpenO)]^{2+}$ are transformed into two diastereoisomers of $[Fe^{III}(OOH)(HtpenO)]^{2+}$.

The addition of Et_3N to a solution of $[Fe^{III}(OOH)(HtpenO)]^{2+}$ results in deprotonation of the hydroperoxo ligand to generate the green side-on peroxo bound species $[Fe^{III}(OO)(HtpenO)]^+$ (λ_{max} = 713 nm).[52] This is formed directly on the addition of excess (30 equiv) H_2O_2 to $[Fe^{III}(tpenO)]^{2+}$ under marginally basic conditions. Like the other iron hydroperoxides supported by ethylenediamine-backboned Rtpen ligand systems, this is a high-spin iron(III) complex ($S = 5/2$, g^{eff} = 8.0, 4.3). The Fe–O and O–O vibrational bands are observed at 472 and 818 cm^{-1}, respectively (Figure 4a, green). The end-on hydroperoxo and the side-on peroxide complexes supported by HtpenO show longer lifetimes than the corresponding complexes supported by Htpena[46] but shorter lifetimes than the corresponding complexes supported by Rtpen[52] and Htpen. At -15 °C the $T_{1/2}$ value is 30 min for $[Fe^{III}(OO)(HtpenO)]^+$ (10 equiv of Et_3N, 50 equiv of H_2O_2).

Oxidative Transformation of tpenO to tpena. The chemical robustness of $[Fe^{III}(tpenO)]^{2+}$ strongly depends on the number of equivalents of H_2O_2 and base added. Investigation of MeOH solutions of $[Fe^{III}(tpenO)]^{2+}$ aged for 1 h after the reaction with 50 equiv of H_2O_2 with EPR spectroscopy shows that the two diastereoisomers of $[Fe^{III}(tpenO)]^{2+}$ exist in a ratio similar to that before the reaction with H_2O_2 (Figure S5). Consistently investigation of exactly the same sample as used for the EPR experiment with ESI-MS shows the base peak at m/z 432 corresponding to $[Fe^{II}(tpenO)]^+$ as was present before the reaction with H_2O_2; however, a new abundant ion at m/z 446 (25%) has appeared. This can be assigned to $[Fe^{II}(tpena)]^+$ (Figure 5a). When 100 equiv of of H_2O_2 was added to $[Fe^{III}(tpenO)]^{2+}$, the peak at m/z 432 is completely absent and m/z 446 becomes the base peak of the spectrum. These results indicate that the methylene group of the alkoxide group is easily oxidized, in situ, to a carboxylate group and therewith transforming tpenO into tpena (Scheme 4). The ligand transformation is even more pronounced in the presence of base, and the conversion was followed also with time-dependent UV/vis spectroscopy. When <10 equiv of Et_3N was added to deprotonate $[Fe^{III}(OOH)(HtpenO)]^{2+}$ to give $[Fe^{III}(OO)(HtpenO)]^{2+}$ (λ_{max} 713 nm), $[Fe^{III}(OOH)(HtpenO)]^{2+}$ could be regenerated by the addition of a second portion of H_2O_2 (50 equiv). When, however, more than 30 equiv of base was added to $[Fe^{III}(OOH)(HtpenO)]^{2+}$ in methanol, a blue shift of the absorbance band from λ_{max} = 713 nm to λ_{max} = 675 nm occurred before its complete disappearance within seconds at -30 °C (Figure 5b). The final absorption spectrum is consistent with λ_{max} = 675 nm recorded for $[Fe^{III}(OO)(Htpena)]^+$ in acetonitrile (Scheme 4).[46] In the absence of other substrates $[Fe^{III}(OO)(Htpena)]^+$ is prone to oxidative destruction in the presence of small amounts of H_2O_2 (i.e., concentrations at which H_2O_2 disproportionation is outcompeted by intra- and intermolecular HAT) even at -30 °C.[46] Consistently absolute intensities of the ions in the ESI-MS spectra of aged samples of $[Fe^{III}(OO)(HtpenO)]^+$ (50 equiv of H_2O_2, 30 equiv of Et_3N) are extremely weak, supporting total degradation of the newly formed tpena (Figure S6). Titration with just 1 or 2 equiv of Et_3N demonstrated that the abundance of $[Fe^{II}(tpena)]^+$ (m/z 446.12) in comparison to that of $[Fe^{II}(tpenO)]^+$ (m/z 432.15) increases as base is added (Figure S7). This suggests that either $[Fe^{III}(OO)(Htpena)]^+$ is more reactive than $[Fe^{III}(OOH)(HtpenO)]^{2+}$ or that the conversion of HtpenO to Htpena
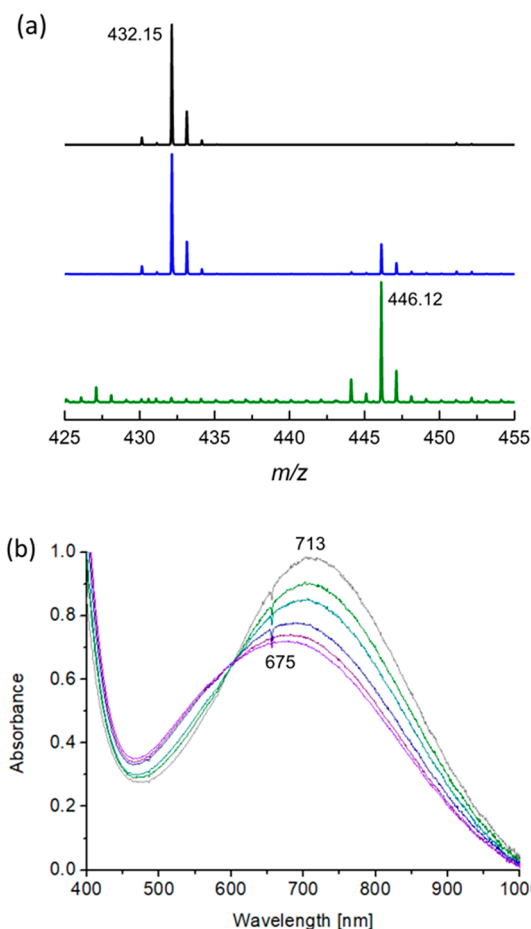
Figure 5. (a) H_2O_2-dependent ESI-MS spectra of $[Fe^{II}Cl(tpenOH)]$-PF_6 in MeOH: 0 equiv of H_2O_2 (black), 50 equiv of H_2O_2 (blue), and 100 equiv of H_2O_2 (green). Assignment: m/z 432.15, $[Fe^{II}(tpenO)]^+$; 446.12, $[Fe^{II}(tpena)]^+$. (b) Conversion of $[Fe^{III}(OO)(HtpenO)]^+$ to $[Fe^{III}(OO)(Htpena)]^+$ over 1 min at $-30\ °C$ (50 equiv of H_2O_2, 30 equiv of Et_3N, $[Fe] = 1\ mM$).

Scheme 4. Regioselective Ligand Oxidation of HtpenO to Htpena in Iron(III) Peroxide Complexes
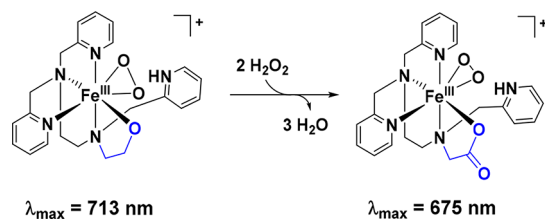
includes a step in the reaction pathway which is assisted by the presence of base.

Trends in Oxidative Potency of Solutions of $[Fe^{III}(tpen)]^{3+}$, $[Fe^{III}(tpenO)]^{2+}$, and $[Fe^{III}(tpena)]^{2+}$ and H_2O_2. Iron(III) hydroperoxide complexes decay to an iron(IV) oxo or occasionally an iron(V) oxo complex by O–O homolysis and heterolysis,[58,59] respectively. Our original motivation for this work was a search for a rare positively charged iron(V) oxo complex. The presence of a cis-alkoxo or -carboxylato donor in an ethylenediamine-based ligand could conceivably produce this by a heterolytic $Fe^{III}O$–OH cleavage. Our observations, however, are most consistent with a homolytic mechanism (eq 2) for all the systems studied here.

$$[LFe^{III}OOH]^{n+} \rightarrow [LFe^{IV}O]^{n+} + {}^{\bullet}OH \qquad (2)$$
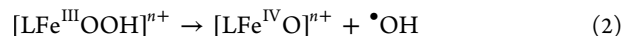
There has been some tendency in the literature to assign reactivity in substrate oxidation solely to the iron-based oxidants. In the case of generation of iron(IV) oxo via iron(III) hydroperoxides this potentially means that the concurrent production of aggressively oxidizing hydroxyl radicals has sometimes been overlooked. These can also engage in H atom abstracting reactions. The most appropriate assessment of the catalytic C–H oxidizing power was therefore to study mixtures containing the terminal oxidant H_2O_2 and the same concentration of either $[Fe^{II}(tpen)]^{2+}$, $[Fe^{III}(tpenO)]^{2+}$, or $[Fe^{III}(tpena)]^{2+}$ or iron perchlorate salts. This enables comparison of the chemistries of the oxidative mixtures without attribution of the "direct" oxidizing power to a particular single species (H_2O_2, iron(III) (hydro)peroxide, iron(III) hydroxo, iron(IV) oxo, or ${}^{\bullet}OH$). It should be mentioned, however, that the reactivities of $[Fe^{III}OOH(L)]^{2+}$ and $[Fe^{IV}O(L)]^{2+}$ complexes supported by tetradentate N4 ligand scaffolds (L = bztpen, TPA, TMC, N4Py; N4Py = N,N-bis(2-pyridylmethyl)-N-bis(2-pyridyl)methylamine) toward substrate C–H oxidation have been compared with the conclusion that the iron(IV) oxo complexes are stronger oxidants than the parent iron(III) hydroperoxides.[60,61] As described above, there is a clear difference in the amount of methanol (C–H BDE = 96.1 kcal mol^{-1} [62]) oxidation that occurs in these mixtures, with a significantly larger production of formaldehyde for the $[Fe^{III}(tpena)]^{2+}$-catalyzed reactions in comparison to those catalyzed by $[Fe^{III}(tpenO)]^{2+}$ and $[Fe^{II}(tpen)]^{2+}$. We turned therefore to a more challenging C–H substrate, cyclohexane (C–H BDE = 99.5 kcal mol^{-1} [62]) to evaluate the potency of the catalytic mixtures. Cyclohexanol and cyclohexanone were detected (GC) as the only products (Table 2).

The oxidation of cyclohexane to cyclohexanol can be initiated by a HAT reaction. Two oxidants are the most

Table 2. Comparison of Product Distribution during the Oxidation of Cyclohexane[a]

| solid precatalyst | dominant solution state speciation (excluding H_2O_2 adducts) | product (mM) | | ketone:alcohol |
		cyclohexanone	cyclohexanol	
no catalyst		0.0(0)	0.0(0)	
$Fe(ClO_4)_2 \cdot 6H_2O$	$[Fe(H_2O)_6]^{2+}$	0.0(0)	0.0(0)	
$Fe(ClO_4)_3 \cdot 6H_2O$	$[Fe(H_2O)_6]^{3+}$, $[Fe_2(O)(H_2O)_{10}]^{4+}$	0.0(0)	4.0(4)	
$[Fe(tpen)](PF_6)_2$	$[Fe^{II}(tpen)]^{2+}$	3.4(2)	5.3(2)	1:1.5
$[FeCl(tpenOH)]PF_6$	$[Fe^{III}(tpenO)]^{2+}$	3.2(2)	3.9(3)	1:1.2
$[Fe_2O(Htpena)_2](ClO_4)_4$	$[Fe^{III}(tpena)]^{2+}$	3.1(2)	10.6(3)	1:3.4

[a]Reaction conditions: [Fe] (1 mM), cyclohexane (500 mM) and H_2O_2 (100 mM) in 2 mL of MeCN (C–H BDE = 97.0 kcal mol^{-1} [62]) at room temperature in air. The reported values represent an average of four runs.

plausible for this, an iron(IV) oxo or the $^{\bullet}$OH radical. This is followed by a radical termination with a hydroxyl radical (Scheme 5a). The oxidation of cyclohexanol to cyclohexanone

Scheme 5. (a) Oxidation of Cyclohexane to Cyclohexanol, (b) Iron(IV) Oxo Mediated Oxidation of Cyclohexanol to Cyclohexanone, (c) Oxygen-Dependent Formation of Cyclohexanone, and (d) Generation of HOO$^{\bullet}$
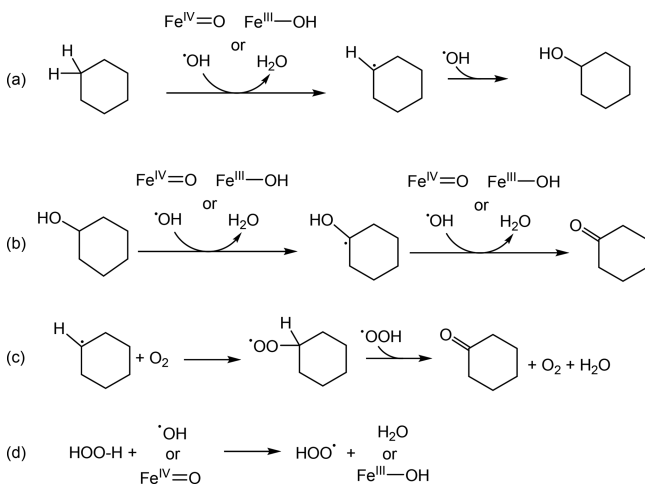
is also a two-electron process which can occur by two consecutive iron(IV) oxo mediated HAT reactions (Scheme 5b). Alternatively, cyclohexanone can be formed using O_2 if an H atom has been abstracted from cyclohexanol (Scheme 5c). Subsequent reaction of the organoperoxy radical with a hydroperoxy radical (in turn generated by H atom abstraction from H_2O_2 by $^{\bullet}$OH radical or an iron(IV) oxo, Scheme 5d) will cascade into the ketone product. It has been shown that protection of the catalytic experiments from O_2 lowers the yield of the ketone product.[63,64] It was not possible in the present study to probe this because H_2O_2 disproportionation is a competing reaction in the presence of $[Fe^{III}(tpena)]^{2+}$.[46] This competing H_2O_2 disproportionation was minimized by slow addition of H_2O_2 with a syringe pump and a large excess of substrate (Fe:H_2O_2:cyclohexane = 1:100:500). All three catalysts showed similar yields of cyclohexanone. No cyclohexanone was detected using iron(II)/(III) perchlorates.

In the presence of the simple iron(III) salt Fe(ClO$_4$)$_3$, it was interesting to see that low yields of cyclohexanol were obtained and these yields are comparable to those when precatalysts $[Fe^{II}Cl(tpenOH)]PF_6$ and $[Fe^{II}(tpen)](PF_6)_2$ are used. Groves and Van Der Puy[65,66] as well as Sawyer and Sugimoto[67,68] have previously shown that simple iron salts such as Fe(ClO$_4$)$_{2/3}$ and FeCl$_3$ can catalyze the oxidation of simple organic compounds using H_2O_2 as the oxidant. Pronounced regio- and stereoselectivity were reported and interpreted as evidence for the generation and involvement of a metal-bound oxidant, proposed to be the ferryl ion intermediate, FeO^{2+} (sic). The important message in our data is that $[Fe^{III}(tpena)]^{2+}$-catalyzed reactions show twice the yield of cyclohexanol product in comparison to the reactions catalyzed by $[Fe^{III}(tpen)]^{2+}$ and $[Fe^{III}(tpenO)]^{2+}$. This indicates an enhanced reactivity in HAT reactions toward the strong C–H bonds in cyclohexane. The reaction using $[Fe^{III}(tpenO)]^{2+}$ as a catalyst gives the lowest yield of cyclohexanol. This stands in contrast to the results on the catalytic oxidation of methanol to formaldehyde, where

$[Fe^{III}(tpenO)]^{2+}$ outperformed $[Fe^{II}(tpen)]^{2+}$ as a catalyst. This can be rationalized by the fact that the oxidation of the alkoxide arm of tpenO in $[Fe^{III}(tpenO)]^{2+}$ is likely to be more pronounced when it is in competition with cyclohexane (in MeCN) as a substrate. The consequence will be a change in the order of potency of the iron complexes as catalysts. Given that the background $^{\bullet}$OH radical concentration will be the same in all reactions, and presuming that the iron hydroperoxides are not active as the direct oxidants,[60,61] then it can be concluded that $[Fe^{IV}O(Htpena)]^{2+}$ is the most potent iron(IV) oxo species in this series and is consistent with the oxidation of cyclohexanol in water using $[Fe^{IV}O(Htpena)]^{2+}$ generated by electroactivation where no $^{\bullet}$OH radicals are present.[50] Thus, both experiments point to $[Fe^{IV}O(Htpena)]^{2+}$ as a catalytically competent oxidant with significant radical character. Crucially, the chemistry we have observed is consistent with $[Fe^{III}(OOH)(Htpena)]^{2+}$ showing a relatively rapid cleavage of the O–O bond relative to the other two iron(III) hydroperoxides. While we have not been able to measure this directly due to transiency, we have achieved this for the analogue $[Fe^{III}(OO^tBu)(Htpena)]^{2+}$ in MeCN. Here we were able to show that $[Fe^{IV}O(Htpena)]^{2+}$ is the direct product of rapid homolytic FeO–O^{t}Bu cleavage.[69] We can conclude from all the observations that the latent iron(IV)oxo complex of tpena is more rapidly available, in higher concentrations, in comparison with the tpen- and tpenO-supported systems in the presence of H_2O_2.

■ CONCLUSION

There is a paucity of iron complexes with chelating ligands containing O atom donors that can activate H_2O_2, despite their relevance to the carboxylate (Glu, Asp) donors at the active site of nonheme enzymes. $[Fe^{III}(tpena)]^{2+}$ and $[Fe^{III}(tpenO)]^{2+}$ fill this gap in the literature. They show redox and reactivity patterns distinct from their sister, $[Fe^{II}(tpen)]^{2+}$. Using this geometrically matched set of compounds, we can confirm that the presence of an oxygen atom in the first coordination sphere reduces the Fe^{II} to Fe^{III} oxidation potentials, as might be expected. The carboxylato donor does this by 350 mV and the alkoxido donor by 470 mV in comparison to the pyridine donor. This is in accord with the fact that iron(III) complexes have so far been isolated using the tpena ligand.[46–48] For tpen iron(II) complexes are the most facile to isolate.[53,70] The situation is more complicated for tpenOH due to solvent and anion dependence. The one known structurally characterized complex is $[Fe^{II}Cl(tpenOH)]PF_6$.[52] In this the ligand is not hexadentate because the ethanol arm is uncoordinated. In methanol solution, however, $[Fe^{II}Cl(tpenOH)]^+$ is spontaneously air oxidized to $[Fe^{III}(tpenO)]^{2+}$ and this is accompanied by a switch from pentadentate N5 to hexadentate N5O coordination for the ligand. EPR spectroscopy indicates that both the *mer* and *fac* diastereoisomers of $[Fe^{III}(tpenO)]^{2+}$ (Scheme 2d) show low-spin ground states. The methylene group of the alkoxide of tpenO is a vulnerable site for oxidation, and it undergoes a selective oxidation to generate tpena in the presence of H_2O_2.

The iron complexes of the potentially hexadentate ethylenediamine-based ligands described here stand out with respect to most other models for nonheme iron that have been constructed using tetra- and pentadentate ligands: All three complexes, in their +3 oxidation state, rapidly form a spectroscopically identified "charge-separated" adduct with H_2O_2, where the base for its deprotonation is internally

Table 3. Electrochemical and H_2O_2 Activation Properties of the Iron Complexes of Ethylenediamine-Based N6 and N5O Ligands[a]

	Fe^{III}/Fe^{II} redox potential vs Fc$^+$/Fc (V)	solvent for observation of hydroperoxide adduct[b]	catalysis		
			converion for MeOH oxidation[c]	product ratio (cyclohexanone/cyclohexanol) for cyclohexane oxidation[d]	H_2O_2 disproportionation[e]
[Fe^{II}(tpen)]$^{2+,f}$	0.39[g]	MeOH	2%	1:1.5	no
[Fe^{III}(tpena)]$^{2+}$	0.04[g]	MeCN	35%	1:3.4	yes
[Fe^{III}(tpenO)]$^{2+}$	−0.08[h]	MeOH	8%	1:1.2	no

[a]All experiments were performed at room temperature. [b][Fe] = 0.5 mM, 50 equiv of H_2O_2. [c][Fe] = 1.5 mM, 50 equiv of H_2O_2. Reaction time 15 min. Quantification of methanol to formaldehyde was performed colorimetrically.[57] [d][Fe] = 1 mM, cyclohexane 500 mM, H_2O_2 100 mM, solvent MeCN. [e][Fe] = 0.5 mM in MeCN, 50 equiv of H_2O_2. [f]We have not performed the entire set of experiment using the N5 Rtpen (R = Me, Et, iPr, Bz, Ph) supported iron complexes; however, experience[46,52] and spot checks indicate that the H_2O_2 activation chemistry of these systems would be analogous to that of [Fe^{II}(tpen)]$^{2+}$. [g]In MeCN. [h]In MeOH.

provided by a pyridyl arm. This decoordinates and is protonated under ambient conditions. The H_2O_2 adducts of [Fe^{III}(tpen)]$^{3+}$, [Fe^{III}(tpena)]$^{2+}$, and [Fe^{III}(tpenO)] can form without the time-consuming preoxidation step needed when the solution-state precursor complex is [Fe^{II}(tpen)]$^{2+}$.[52] The greater stability of the +3 oxidation state precursors for the N5O ligand supported systems translates into a higher level of O−O bond lability (activation) in the product hydroperoxide complex. Both [Fe^{III}(tpena)]$^{2+}$ and [Fe^{III}(tpenO)]$^{2+}$ catalytically oxidize methanol in the presence of H_2O_2. The complexes based on N-donor-only scaffolds, [Fe^{III}OOH(tpenH)]$^{3+}$ and [Fe^{III}OOH(Rtpen)]$^{2+}$ (R = Me, Et, iPr, Bz, Ph),[52] are on the other hand sluggish oxidants, explaining their ready observation in methanol. Despite its increased transience in comparison to the N-only ligands [Fe^{III}(OOH)(HtpenO)]$^{2+}$ and its conjugate base, [Fe^{III}(OO)(HtpenO)]$^+$ can be spectroscopically detected in methanol with lifetimes of seconds (in the presence of 50 equiv of H_2O_2, at room temperature). [Fe^{III}(OOH)(Htpena)]$^{2+}$ and [Fe^{III}(OO)(Htpena)]$^+$, however, cannot.[46] This corroborates the more effective catalysis of the oxidation of methanol by [Fe^{III}(tpena)]$^{2+}$ that was independently verified by measurement of formaldehyde production. In stark contrast, [Fe^{III}(OOH)(Htpen)]$^{3+}$ and [Fe^{III}(OO)(Htpen)]$^{2+}$ show lifetimes of minutes to hours under the same conditions in methanol, indicating the fact that they cannot directly, or indirectly via daughter high-valent species, oxidize this solvent effectively. All three complexes can oxidize the C−H bond of cyclohexane to a final product of cyclohexanone; however, the detection of greater amounts of intermediate cyclohexanol indicates higher HAT activity for solutions containing [Fe^{III}(tpena)]$^{2+}$ with H_2O_2. Table 3 summarizes the contrasting electrochemical and H_2O_2 activation properties of the iron complexes of ethylenediamine-based N6 and N5O ligands.

Our work establishes the importance of stabilizing higher iron oxidation states to afford more reactive catalysts for substrate oxidation reactions (+3 vs +2). The introduction of one anionic oxygen donor into an otherwise neutral N-only donor set of the endogenous chelating ligands achieves this. Unexpectedly, there are marked contrasts in the H_2O_2 activation chemistries of the alkoxido and carboxylato analogues [Fe^{III}(tpenO)]$^{2+}$ and [Fe^{III}(tpena)]$^{2+}$ with the latter producing an iron(IV) oxo derivative that shows a greater activity in HAT reactions. This does not correlate with the Fe^{III}/Fe^{II} redox potentials of [Fe^{III}(tpenO)]$^{2+}$ and [Fe^{III}(tpena)]$^{2+}$, implying perhaps a role for the biomimetic

carboxylate donor beyond just the stabilization of higher iron oxidation states.

EXPERIMENTAL SECTION

[Fe^{II}(tpen)](PF$_6$)$_2$, [Fe$^{III}_2$O(Htpena)$_2$](ClO$_4$)$_4$, and [Fe^{II}Cl(tpenOH)]PF$_6$ were synthesized as previously described.[47,52,53] H_2O_2 (50% in water, v/v) and all other chemicals were commercially available and used without further purification.

Caution! Perchlorate salts of metal complexes are potentially explosive and should be handled with caution in small quantities.

Generation of [Fe^{III}(OOH)(HtpenO)]$^{2+}$ and [Fe^{III}(OO)-(HtpenO)]$^+$. [Fe^{II}Cl(tpenOH)]PF$_6$ was dissolved in MeOH, and 50 equiv of H_2O_2 was added to generate [Fe^{III}(OOH)(HtpenO)]$^{2+}$. Addition of 10 equiv of Et$_3$N deprotonates the transient species to form [Fe^{III}(OO)(HtpenO)]$^+$. The base can also be added prior to H_2O_2 to form [Fe^{III}(OO)(HtpenO)]$^+$ instantly.

Conversion of [Fe^{III}(OO)(HtpenO)]$^+$ to [Fe^{III}(OO)(Htpena)]$^+$ followed by UV/Vis. H_2O_2 (50 equiv) was added at −30 °C to [Fe^{II}Cl(tpenOH)]PF$_6$ (1 mM) dissolved in MeOH to give [Fe^{III}(OOH)(HtpenO)]$^{2+}$. Et$_3$N (30 equiv) was then added to generate [Fe^{III}(OO)(HtpenO)]$^+$. Over the course of 1 min this undergoes conversion to [Fe^{III}(OO)(Htpena)]$^+$.

Instrumentation and Methods. UV/vis spectra were recorded in 1 cm quartz cuvettes on either an Agilent 8453 spectrophotometer with a UNISOKU CoolSpeK UV USP-203 temperature controller or with an Analytikjena Specord S600 instrument with a Quantum Northwest TC 125 temperature controller. IR spectra were either recorded in the solid state on a Spectrum 65 FT-IR spectrometer (ATR mode, PerkinElmer) or in the solution state on a ChiralIR-2X spectrometer (BioTools). Raman spectra were recorded in 1 cm quartz cuvettes at 785 nm with either a RamanFlex instrument (PerkinElmer) equipped with an Inphotonics industrial probe or a free space laser (75 mW, Ondax, with a 785 nm laser line clean up filter) and collected in backscattering (180°) mode with a Semrock dichroic beamsplitter and a 25 mm diameter/7.5 cm planoconvex lens to focus the laser on the sample and collect the Raman scattering. The Raman scattering was passed through a long-pass filter (Semrock) , focused into a Shamrock300 spectrograph (ANDOR technology), and dispersed onto a iDUS-420-BUEX2 CCD camera. Spectra were calibrated with MeCN/toluene (50/50 v/v). The solutions were cooled with a Quantum Northwest TC 125 temperature controller, and the spectra were obtained at −25 °C. Baseline correction was performed for all spectra and normalized to the solvent band at 1038 cm^{-1}. EPR spectra (X-band) were recorded on a Bruker EMX Plus CW spectrometer (modulation amplitude 10 G, attenuation 10 dB) on frozen solutions at 100 K. Eview4wr and esimX were used for simulation.[71] Cyclic voltammetry was performed on an Eco Chemie Autolab PGSTAT10 Potentiostat/Galvanostat using a standard three-electrode setup with a Pt disk as working electrode, a Pt wire as counter electrode, and Ag/Ag$^+$ as reference electrode (0.01 M AgNO$_3$ in 0.1 M TBAClO$_4$ in MeCN or 0.01 M AgNO$_3$ in 0.1 M TBAClO$_4$ in MeOH; TBA = *tert*-butylammonium). The electrolyte was either 0.1

M TBAClO$_4$ in acetonitrile or 0.1 M TBAClO$_4$ in methanol. The working electrode was cleaned by polishing with 0.05 μm alumina followed by sonication, and the solutions were purged with nitrogen prior to measurements. The oxidation potential of Fc/Fc$^+$ against Ag/Ag$^+$ was measured to be 0.08 V, and all oxidation potentials were converted accordingly. GC analysis was performed using a Hewlett-Packard 6890 Series gas chromatograph system with a flame ionization detector. Values reported are an average of four runs.

Catalysis. H$_2$O$_2$ (100 mM, 440 μL, 1.25%) was slowly added using a syringe pump to 2 mL acetonitrile solutions of the iron catalysts (1 mM [Fe]) and cyclohexane (500 mM) over 20 min at room temperature. The reaction mixture was stirred for an additional 10 min before it was quenched with Al$_2$O$_3$. The solution was filtered, and biphenyl was subsequently added as an internal standard for GC analysis.

■ ASSOCIATED CONTENT

ⓢ Supporting Information

The Supporting Information is available free of charge on the ACS Publications website at DOI: 10.1021/acs.inorg-chem.9b00247.

Time-resolved UV/vis, EPR spectra, CV of [FeCl-(tpenOH)]PF$_6$ in MeOH and MeCN, and Et$_3$N- and/or H$_2$O$_2$-dependent ESI-MS (PDF)

■ AUTHOR INFORMATION

Corresponding Author

*C.J.M.: e-mail, mckenzie@sdu.dk; tel, +45 6550 2518.

ORCID ⓘ

Christina Wegeberg: 0000-0002-6034-453X
Wesley R. Browne: 0000-0001-5063-6961
Christine J. McKenzie: 0000-0001-5587-0626

Notes

The authors declare no competing financial interest.

■ ACKNOWLEDGMENTS

■ REFERENCES

(1) Dudev, T.; Lim, C. Metal Binding Affinity and Selectivity in Metalloproteins: Insights from Computational Studies. *Annu. Rev. Biophys.* **2008**, *37*, 97−116.

(2) Tomchick, D. R.; Phan, P.; Cymborowski, M.; Minor, W.; Holman, T. R. Structural and Functional Characterization of Second-Coordination Sphere Mutants of Soybean Lipoxygenase-1†. *Biochemistry* **2001**, *40* (25), 7509−7517.

(3) Dudev, T.; Lin, Y.; Dudev, M.; Lim, C. First-second Shell Interactions in Metal Binding Sites in Proteins: a PDB Survey and DFT/CDM Calculations. *J. Am. Chem. Soc.* **2003**, *125* (10), 3168−3180.

(4) Zhu, W.; Richards, N. G. J. Biological Functions Controlled by Manganese Redox Changes in Mononuclear Mn-dependent Enzymes. *Essays Biochem.* **2017**, *61* (2), 259−270.

(5) Borovik, A. S. Bioinspired Hydrogen Bond Motifs in Ligand Design: The Role of Noncovalent Interactions in Metal Ion Mediated Activation of Dioxygen. *Acc. Chem. Res.* **2005**, *38* (1), 54−61.

(6) Shook, R. L.; Borovik, A. S. The Effects of Hydrogen Bonds on Metal-mediated O$_2$ Activation and Related Processes. *Chem. Commun.* **2008**, No. 46, 6095−6107.

(7) Shook, R. L.; Borovik, A. S. Role of the Secondary Coordination Sphere in Metal-mediated Dioxygen Activation. *Inorg. Chem.* **2010**, *49* (8), 3646−3660.

(8) Cook, S. A.; Borovik, A. S. Molecular Designs for Controlling the Local Environments Around Metal Ions. *Acc. Chem. Res.* **2015**, *48* (8), 2407−2414.

(9) Cook, S. A.; Hill, E. A.; Borovik, A. S. Lessons from Nature: A Bio-Inspired Approach to Molecular Design. *Biochemistry* **2015**, *54* (27), 4167−4180.

(10) Yosca, T. H.; Behan, R. K.; Krest, C. M.; Onderko, E. L.; Langston, M. C.; Green, M. T. Setting an Upper Limit on the Myoglobin iron(IV)hydroxide pK(a): Insight into Axial Ligand Tuning in Heme Protein Catalysis. *J. Am. Chem. Soc.* **2014**, *136* (25), 9124−9131.

(11) Onderko, E. L.; Silakov, A.; Yosca, T. H.; Green, M. T. Characterization of a Selenocysteine-ligated P450 Compound I Reveals Direct Link Between Electron Donation and Reactivity. *Nat. Chem.* **2017**, *9* (7), 623−628.

(12) Yosca, T. H.; Ledray, A. P.; Ngo, J.; Green, M. T. A New Look at the Role of Thiolate Ligation in Cytochrome P450. *JBIC, J. Biol. Inorg. Chem.* **2017**, *22* (2−3), 209−220.

(13) Pulver, S.; Froland, W. A.; Fox, B. G.; Lipscomb, J. D.; Solomon, E. I. Spectroscopic Studies of the Coupled Binuclear Non-heme Iron Active Site in the Fully Reduced Hydroxylase Component of Methane Monooxygenase: Comparison to Deoxy and Deoxy-azide Hemerythrin. *J. Am. Chem. Soc.* **1993**, *115* (26), 12409−12422.

(14) Wei, P.-P.; Skulan, A. J.; Wade, H.; DeGrado, W. F.; Solomon, E. I. Spectroscopic and Computational Studies of the de Novo Designed Protein DF2t: Correlation to the Biferrous Active Site of Ribonucleotide Reductase and Factors That Affect O2 Reactivity. *J. Am. Chem. Soc.* **2005**, *127* (46), 16098−16106.

(15) Holmes, M. A.; Le Trong, I.; Turley, S.; Sieker, L. C.; Stenkamp, R. E. Structures of Deoxy and Oxy Hemerythrin at 2.0 Å Resolution. *J. Mol. Biol.* **1991**, *218* (3), 583−593.

(16) Rosenzweig, A. C.; Frederick, C. A.; Lippard, S. J.; Nordlund, P. Crystal Structure of a Bacterial Non-haem Iron Hydroxylase That Catalyses the Biological Oxidation of Methane. *Nature* **1993**, *366* (6455), 537−543.

(17) Stenkamp, R. E. Dioxygen and Hemerythrin. *Chem. Rev.* **1994**, *94* (3), 715−726.

(18) Nesheim, J. C.; Lipscomb, J. D. Large Kinetic Isotope Effects in Methane Oxidation Catalyzed by Methane Monooxygenase: Evidence for C−H Bond Cleavage in a Reaction Cycle Intermediate. *Biochemistry* **1996**, *35* (31), 10240−10247.

(19) Shu, L.; Nesheim, J. C.; Kauffmann, K.; Münck, E.; Lipscomb, J. D.; Que, L. An Fe$_2^{IV}$O$_2$ Diamond Core Structure for the Key Intermediate Q of Methane Monooxygenase. *Science* **1997**, *275* (5299), 515−518.

(20) Brazeau, B. J.; Lipscomb, J. D. Kinetics and Activation Thermodynamics of Methane Monooxygenase Compound Q Formation and Reaction with Substrates†. *Biochemistry* **2000**, *39* (44), 13503−13515.

(21) Banerjee, R.; Proshlyakov, Y.; Lipscomb, J. D.; Proshlyakov, D. A. Structure of the Key Species in the Enzymatic Oxidation of Methane to Methanol. *Nature* **2015**, *518* (7539), 431−434.

(22) Castillo, R. G.; Banerjee, R.; Allpress, C. J.; Rohde, G. T.; Bill, E.; Que, L.; Lipscomb, J. D.; DeBeer, S. High-Energy-Resolution Fluorescence-Detected X-ray Absorption of the Q Intermediate of Soluble Methane Monooxygenase. *J. Am. Chem. Soc.* **2017**, *139* (49), 18024−18033.

(23) Kovaleva, E. G.; Lipscomb, J. D. Versatility of Biological Non-heme Fe(II) Centers in Oxygen Activation Reactions. *Nat. Chem. Biol.* **2008**, *4* (3), 186−193.

(24) Kal, S.; Que, L. Dioxygen Activation by Nonheme Iron Enzymes with the 2-His-1-carboxylate Facial Triad That Generate High-valent Oxoiron Oxidants. *JBIC, J. Biol. Inorg. Chem.* **2017**, *22* (2−3), 339−365.

(25) Price, J. C.; Barr, E. W.; Tirupati, B.; Bollinger, J. M.; Krebs, C. The First Direct Characterization of a High-valent Iron Intermediate

in the Reaction of an Alpha-ketoglutarate-dependent Dioxygenase: a High-spin FeIV Complex in Taurine/alpha-ketoglutarate Dioxygenase (TauD) from Escherichia Coli. *Biochemistry* **2003**, *42* (24), 7497−7508.

(26) Riggs-Gelasco, P. J.; Price, J. C.; Guyer, R. B.; Brehm, J. H.; Barr, E. W.; Bollinger, J. M.; Krebs, C. EXAFS Spectroscopic Evidence for an Fe=O Unit in the Fe(IV) Intermediate Observed During Oxygen Activation by Taurine:alpha-ketoglutarate Dioxygenase. *J. Am. Chem. Soc.* **2004**, *126* (26), 8108−8109.

(27) Price, J. C.; Barr, E. W.; Glass, T. E.; Krebs, C.; Bollinger, J. M. Evidence for Hydrogen Abstraction from C1 of Taurine by the High-spin Fe(IV) Intermediate Detected During Oxygen Activation by Taurine:alpha-ketoglutarate Dioxygenase (TauD). *J. Am. Chem. Soc.* **2003**, *125* (43), 13008−13009.

(28) Bollinger, J. M.; Price, J. C.; Hoffart, L. M.; Barr, E. W.; Krebs, C. Mechanism of Taurine: α-Ketoglutarate Dioxygenase (TauD) from Escherichia Coli. *Eur. J. Inorg. Chem.* **2005**, *2005* (21), 4245−4254.

(29) de Groot, J. J.; Veldink, G. A.; Vliegenthart, J. F.; Boldingh, J.; Wever, R.; van Gelder, B. F. Demonstration by EPR Spectroscopy of the Functional Role of Iron in Soybean Lipoxygenase-1. *Biochim. Biophys. Acta* **1975**, *377* (1), 71−79.

(30) Scarrow, R. C.; Trimitsis, M. G.; Buck, C. P.; Grove, G. N.; Cowling, R. A.; Nelson, M. J. X-ray Spectroscopy of the Iron Site in Soybean Lipoxygenase-1: Changes in Coordination Upon Oxidation or Addition of Methanol. *Biochemistry* **1994**, *33* (50), 15023−15035.

(31) Newcomer, M. E.; Brash, A. R. The Structural Basis for Specificity in Lipoxygenase Catalysis. *Protein Sci.* **2015**, *24* (3), 298−309.

(32) Elkins, J. M.; Ryle, M. J.; Clifton, I. J.; Dunning Hotopp, J. C.; Lloyd, J. S.; Burzlaff, N. I.; Baldwin, J. E.; Hausinger, R. P.; Roach, P. L. X-ray Crystal Structure of *Escherichia Coli* Taurine/α-Ketoglutarate Dioxygenase Complexed to Ferrous Iron and Substrates[†,‡]. *Biochemistry* **2002**, *41* (16), 5185−5192.

(33) Minor, W.; Steczko, J.; Stec, B.; Otwinowski, Z.; Bolin, J. T.; Walter, R.; Axelrod, B. Crystal Structure of Soybean Lipoxygenase L-1 at 1.4 A Resolution. *Biochemistry* **1996**, *35* (33), 10687−10701.

(34) Namuswe, F.; Kasper, G. D.; Sarjeant, A. A. N.; Hayashi, T.; Krest, C. M.; Green, M. T.; Moënne-Loccoz, P.; Goldberg, D. P. Rational Tuning of the Thiolate Donor in Model Complexes of Superoxide Reductase: Direct Evidence for a Trans Influence in Fe(III)-OOR Complexes. *J. Am. Chem. Soc.* **2008**, *130* (43), 14189−14200.

(35) Lehnert, N.; Ho, R. Y.; Que, L.; Solomon, E. I. Electronic Structure of High-spin iron(III)-alkylperoxo Complexes and Its Relation to Low-spin Analogues: Reaction Coordinate of O-O Bond Homolysis. *J. Am. Chem. Soc.* **2001**, *123* (51), 12802−12816.

(36) Rohde, J.-U.; Stubna, A.; Bominaar, E. L.; Münck, E.; Nam, W.; Que, L. Nonheme oxoiron(IV) Complexes of Tris(2-pyridylmethyl)-amine with Cis-monoanionic Ligands. *Inorg. Chem.* **2006**, *45* (16), 6435−6445.

(37) Jackson, T. A.; Rohde, J.-U.; Seo, M. S.; Sastri, C. V.; DeHont, R.; Stubna, A.; Ohta, T.; Kitagawa, T.; Münck, E.; Nam, W.; et al. Axial Ligand Effects on the Geometric and Electronic Structures of Nonheme oxoiron(IV) Complexes. *J. Am. Chem. Soc.* **2008**, *130* (37), 12394−12407.

(38) Bukowski, M. R.; Comba, P.; Lienke, A.; Limberg, C.; Lopez de Laorden, C.; Mas-Ballesté, R.; Merz, M.; Que, L. Catalytic Epoxidation and 1,2-dihydroxylation of Olefins with bispidine-iron(II)/H₂O₂ Systems. *Angew. Chem., Int. Ed.* **2006**, *45* (21), 3446−3449.

(39) Bukowski, M. R.; Koehntop, K. D.; Stubna, A.; Bominaar, E. L.; Halfen, J. A.; Münck, E.; Nam, W.; Que, L. A Thiolate-ligated Nonheme oxoiron(IV) Complex Relevant to Cytochrome P450. *Science* **2005**, *310* (5750), 1000−1002.

(40) Sastri, C. V.; Lee, J.; Oh, K.; Lee, Y. J.; Lee, J.; Jackson, T. A.; Ray, K.; Hirao, H.; Shin, W.; Halfen, J. A.; et al. Axial Ligand Tuning of a Nonheme iron(IV)-oxo Unit for Hydrogen Atom Abstraction. *Proc. Natl. Acad. Sci. U. S. A.* **2007**, *104* (49), 19181−19186.

(41) Bernal, I.; Jensen, I. M.; Jensen, K. B.; McKenzie, C. J.; Toftlund, H.; Tuchagues, J.-P. Iron(II) Complexes of Polydentate Aminopyridyl Ligands and an Exchangeable Sixth Ligand; Reactions with Peroxides. Crystal Structure of [FeL¹(H₂O)][PF₆]₂ ·H₂O [L¹ = N,N′-bis-(6-methyl-2-pyridylmethyl)-N,N′-bis(2-pyridylmethyl)-ethane-1,2-diamine]. *J. Chem. Soc., Dalton Trans.* **1995**, No. 22, 3667−3675.

(42) Jensen, K. B.; McKenzie, C. J.; Nielsen, L. P.; Zacho Pedersen, J.; Svendsen, H. M. Deprotonation of Low-spin Mononuclear iron(III)−hydroperoxide Complexes Give Transient Blue Species Assigned to High-spin iron(III)−peroxide Complexes. *Chem. Commun.* **1999**, No. 14, 1313−1314.

(43) Mialane, P.; Nivorojkine, A.; Pratviel, G.; Azéma, L.; Slany, M.; Godde, F.; Simaan, A.; Banse, F.; Kargar-Grisel, T.; Bouchoux, G.; et al. Structures of Fe(II) Complexes with N, N, N′-Tris(2-pyridylmethyl)ethane-1,2-diamine Type Ligands. Bleomycin-like DNA Cleavage and Enhancement by an Alkylammonium Substituent on the N′ Atom of the Ligand. *Inorg. Chem.* **1999**, *38* (6), 1085−1092.

(44) Horner, O.; Jeandey, C.; Oddou, J.-L.; Bonville, P.; McKenzie, C.; Latour, J.-M. Hydrogenperoxo-[(bztpen)Fe(OOH)]²⁺ and Its Deprotonation Product Peroxo-[(bztpen)Fe(O₂)]⁺, Studied by EPR and Mössbauer Spectroscopy − Implications for the Electronic Structures of Peroxo Model Complexes. *Eur. J. Inorg. Chem.* **2002**, *2002* (12), 3278−3283.

(45) Nielsen, A.; Larsen, F. B.; Bond, A. D.; McKenzie, C. J. Regiospecific Ligand Oxygenation in Iron Complexes of a Carboxylate-containing Ligand Mediated by a Proposed Fe(V)-oxo Species. *Angew. Chem., Int. Ed.* **2006**, *45* (10), 1602−1606.

(46) Wegeberg, C.; Lauritsen, F. R.; Frandsen, C.; Mørup, S.; Browne, W. R.; McKenzie, C. J. Directing a Non-Heme Iron(III)-Hydroperoxide Species on a Trifurcated Reactivity Pathway. *Chem. - Eur. J.* **2018**, *24* (20), 5134−5145.

(47) Lennartson, A.; McKenzie, C. J. An iron(III) Iodosylbenzene Complex: a Masked Non-heme Fe(V)O. *Angew. Chem., Int. Ed.* **2012**, *51* (27), 6767−6770.

(48) de Sousa, D. P.; Wegeberg, C.; Vad, M. S.; Mørup, S.; Frandsen, C.; Donald, W. A.; McKenzie, C. J. Halogen-Bonding-Assisted Iodosylbenzene Activation by a Homogenous Iron Catalyst. *Chem. - Eur. J.* **2016**, *22* (11), 3810−3820.

(49) Vad, M. S.; Lennartson, A.; Nielsen, A.; Harmer, J.; McGrady, J. E.; Frandsen, C.; Mørup, S.; McKenzie, C. J. An Aqueous Non-heme Fe(IV)oxo Complex with a Basic Group in the Second Coordination Sphere. *Chem. Commun.* **2012**, *48* (88), 10880−10882.

(50) de Sousa, D. P.; Miller, C. J.; Chang, Y.; Waite, T. D.; McKenzie, C. J. Electrochemically Generated cis-Carboxylato-Coordinated Iron(IV) Oxo Acid-Base Congeners as Promiscuous Oxidants of Water Pollutants. *Inorg. Chem.* **2017**, *56* (24), 14936−14947.

(51) Simaan, A. J.; Döpner, S.; Banse, F.; Bourcier, S.; Bouchoux, G.; Boussac, A.; Hildebrandt, P.; Girerd, J.-J. FeᴵᴵᴵHydroperoxo and Peroxo Complexes with Aminopyridyl Ligands and the Resonance Raman Spectroscopic Identification of the Fe−O and O−O Stretching Modes. *Eur. J. Inorg. Chem.* **2000**, *2000* (7), 1627−1633.

(52) Hazell, A.; McKenzie, C. J.; Nielsen, L. P.; Schindler, S.; Weitzer, M. Mononuclear Non-heme Iron(III) Peroxide Complexes: Syntheses, Characterisation, Mass Spectrometric and Kinetic Studies. *J. Chem. Soc., Dalton Trans.* **2002**, No. 3, 310.

(53) Chang, H. R.; McCusker, J. K.; Toftlund, H.; Wilson, S. R.; Trautwein, A. X.; Winkler, H.; Hendrickson, D. N. [Tetrakis(2-pyridylmethyl)ethylenediamine]iron(II) Perchlorate, the First Rapidly Interconverting Ferrous Spin-crossover Complex. *J. Am. Chem. Soc.* **1990**, *112* (19), 6814−6827.

(54) Duelund, L.; Hazell, R.; McKenzie, C. J.; Preuss Nielsen, L.; Toftlund, H. Solid and Solution State Structures of Mono- and Di-nuclear iron(III) Complexes of Related Hexadentate and Pentadentate Aminopyridyl Ligands. *J. Chem. Soc., Dalton Trans.* **2001**, No. 2, 152−156.

(55) Wegeberg, C.; Fernández-Alvarez, V. M.; de Aguirre, A.; Frandsen, C.; Browne, W. R.; Maseras, F.; McKenzie, C. J. Photoinduced O$_2$-Dependent Stepwise Oxidative Deglycination of a Nonheme Iron(III) Complex. *J. Am. Chem. Soc.* **2018**, *140* (43), 14150−14160.

(56) Thibon, A.; Bartoli, J.-F.; Bourcier, S.; Banse, F. Mononuclear Iron Complexes Relevant to Nonheme Iron Oxygenases. Synthesis, Characterizations and Reactivity of Fe-Oxo and Fe-Peroxo Intermediates. *Dalton Trans.* **2009**, No. 43, 9587−9594.

(57) Nash, T. The Colorimetric Estimation of Formaldehyde by Means of the Hantzsch Reaction. *Biochem. J.* **1953**, *55* (3), 416−421.

(58) Hitomi, Y.; Arakawa, K.; Funabiki, T.; Kodera, M. An iron(III)-monoamidate Complex Catalyst for Selective Hydroxylation of Alkane C-H Bonds with Hydrogen Peroxide. *Angew. Chem., Int. Ed.* **2012**, *51* (14), 3448−3452.

(59) Collins, T. J.; Ryabov, A. D. Targeting of High-Valent Iron-TAML Activators at Hydrocarbons and Beyond. *Chem. Rev.* **2017**, *117* (13), 9140−9162.

(60) Park, M. J.; Lee, J.; Suh, Y.; Kim, J.; Nam, W. Reactivities of Mononuclear Non-heme Iron Intermediates Including Evidence That iron(III)-hydroperoxo Species Is a Sluggish Oxidant. *J. Am. Chem. Soc.* **2006**, *128* (8), 2630−2634.

(61) Roelfes, G.; Lubben, M.; Hage, R.; Que, L., Jr.; Feringa, B. L. Catalytic Oxidation with a Non-Heme Iron Complex That Generates a Low-Spin Fe^{III}OOH Intermediate. *Chem.-Eur. J.* **2000**, *6* (12), 2152−2159.

(62) Luo, Y.-R. *Comprehensive Handbook of Chemical Bond Energies*; CRC Press: Boca Raton, FL, 2007.

(63) Kim, J.; Harrison, R. G.; Kim, C.; Que, L. Fe(TPA)-Catalyzed Alkane Hydroxylation. Metal-Based Oxidation Vs Radical Chain Autoxidation. *J. Am. Chem. Soc.* **1996**, *118* (18), 4373−4379.

(64) Arends, I. W. C. E.; Ingold, K. U.; Wayner, D. D. M. A Mechanistic Probe for Oxygen Activation by Metal Complexes and Hydroperoxides and Its Application to Alkane Functionalization by [Fe^{III}Cl$_2$tris(2-pyridinylmethyl)amine]$^+$ BF$_4^-$. *J. Am. Chem. Soc.* **1995**, *117* (16), 4710−4711.

(65) Groves, J. T.; Van der Puy, M. Stereospecific Aliphatic Hydroxylation by an Iron-based Oxidant. *J. Am. Chem. Soc.* **1974**, *96* (16), 5274−5275.

(66) Groves, J. T.; Van der Puy, M. Stereospecific Aliphatic Hydroxylation by Iron-hydrogen Peroxide. Evidence for a Stepwise Process. *J. Am. Chem. Soc.* **1976**, *98* (17), 5290−5297.

(67) Sugimoto, H.; Sawyer, D. T. Iron(II)-induced Activation of Hydrogen Peroxide to Ferryl Ion (FeO^{2+}) and Singlet Oxygen (^{1}O$_2$) in Acetonitrile: Monoxygenations, Dehydrogenations, and Dioxygenations of Organic Substrates. *J. Am. Chem. Soc.* **1984**, *106* (15), 4283−4285.

(68) Sugimoto, H.; Sawyer, D. T. Iron(II)-induced Activation of Hydroperoxides for the Dehydrogenation and Monooxygenation of Organic Substrates in Acetonitrile. *J. Am. Chem. Soc.* **1985**, *107* (20), 5712−5716.

(69) Wegeberg, C.; Browne, W. R.; McKenzie, C. J. Catalytic Alkyl Hydroperoxide and Acyl Hydroperoxide Disproportionation by a Nonheme Iron Complex. *ACS Catal.* **2018**, *8* (11), 9980−9991.

(70) Thibon, A.; Bartoli, J.-F.; Guillot, R.; Sainton, J.; Martinho, M.; Mansuy, D.; Banse, F. Non-heme Iron Polyazadentate Complexes as Catalysts for Aromatic Hydroxylation by H2O2: Particular Efficiency of tetrakis(2-pyridylmethyl)ethylenediamine−iron(II) Complexes. *J. Mol. Catal. A: Chem.* **2008**, *287* (1−2), 115−120.

(71) By E. Bill (Max-Planck-Institute for Chemical Energy Conversion in Mülheim); available from the author by mail to eckhard.bill@cec.mpg.de, 2018.